Mechanical fracture parameters of concrete drill-core specimens supported by a slenderness ratio study

D Lisztwan[1, 3], I Kumpova[2, 3], P Danek[1], P Frantík[2] and Z Kersner[2]

[1] Brno University of Technology, Faculty of Civil Engineering, Institute of Building Testing, Veveri 331/95, 602 00 Brno, Czech Republic
[2] Brno University of Technology, Faculty of Civil Engineering, Institute of Structural Mechanics, Veveri 331/95, 602 00 Brno, Czech Republic
[3] The Institute of Theoretical and Applied Mechanics of the Czech Academy of Sciences, Prosecka 809/76, 190 00 Prague 9, Czech Republic

E-mail: Dominik.Lisztwan@vutbr.cz; Ivana.Kumpova@vutbr.cz

Abstract. The detailed analytical and experimental investigation of the fracture behaviour of quasi-brittle materials is an endeavour which has been ongoing worldwide for many years. Such materials are usually characterized in terms of their mechanical fracture parameters, which are determined based on the evaluation of quasi-static fracture experiments. One of the most commonly used building materials with a quasi-brittle response is concrete, which is most often based on a cement matrix. It is sometimes also necessary to characterize concrete included in existing structures. In this case, test specimens are obtained by core drilling, and the investigation is conducted with the requirement to maximize the number of parameters obtained while minimizing the number of test specimens drilled from the structure. This paper focuses on the mechanical fracture parameters of core-drilled specimens taken from a selected concrete structure. Tests were performed on cylindrical specimens with a chevron-notched stress concentrator in the three-point bending configuration in order to determine modulus of elasticity, fracture toughness and fracture energy. Subsequently, theoretical compressive strength was estimated and tests for the determination of compressive strength values were performed focusing on dependence on the slenderness ratio, i.e. the relationship between the compressive strength and the length to diameter ratio of the cylindrical specimens. In relation to the obtained mechanical fracture parameters, selected specimens were analysed and three-dimensionally characterized via high-resolution X-ray computed tomography.

1. Introduction

The detailed analytical and experimental investigation of the fracture behaviour of quasi-brittle materials is an endeavour which has been ongoing worldwide for many years [1–3]. Materials with a quasi-brittle response are most often characterized in terms of their basic mechanical fracture parameters, which are usually determined based on the evaluation of quasi-static fracture experiments. One of the most commonly used building materials with a quasi-brittle response is concrete, which is most often based on a cement matrix. Concrete test specimens are prepared from the developed concrete mixtures in appropriate mould sand tested at the required stage of maturity, or – as in the case of the presented work – can be obtained from existing structures for the purposes of construction research or the evaluation and specification of load tests to assess their current state. The success of a fracture experiment and the

accuracy of its results depends on several factors: the chosen method of loading (which must be adequate for the needs of the experiment), the determined range of the applied load, and also the selection of suitable measuring methods and equipment along with their most advantageous location on the structure. As regards the computational support for loading experiments, i.e. measuring the deformation of structures, determining the degree of their degradation or estimating their load-bearing capacity, it is necessary to have accurate data on as many input mechanical fracture parameters as possible. At the same time, it is necessary to maximize the amount of obtained parameter values while minimizing the number of test specimens taken from the structure.

The diagnostic analysis and evaluation of existing concrete structures is a very complex discipline. The successful evaluation of the current condition of a structure requires knowledge of the physical and mechanical parameters of the materials from which it is made. In the case of a new structure, the properties of the materials used are defined using specimens made during the construction process itself. When determining the material characteristics of existing structures, one of the few methods that can be used for obtaining specimens is core drilling. The core-drilling method used to collect specimens from concrete structures uses special diamond drill bits, which vary in size (diameter, length). The right choice of drill core size depends on several factors: the size of the structure, the maximum aggregate size, and the importance of preventing damage to the tested structure. The smallest core diameter that can be drilled from a structure is around 25 mm (micro cores). Nevertheless, cores as small as that are used only in special cases. Cores of diameters from 50 to 100 mm are most commonly used, though it is the case that the smaller the core diameter, the less damaging it is to the tested structure [4].

Existing codes and requirements specify the dimensions of specimens that can be used to evaluate the compressive strength of concrete f_c. An important factor which influences the subsequent compressive strength of concrete is the slenderness (L/D ratio) of the tested specimens [5]. Most often, standard specimens (made in a mould) have an L/D ratio of 1.0 (cube strength) or 2.0 (cylinder strength). In this case, some codes allow the compressive strength of the drill-core specimens with an L/D ratio in this range to be transformed into cube or cylinder strength using a correction factor [6].

Structural concrete can be also characterized via parameters obtained via the evaluation of fracture tests, and this paper presents the results of the evaluation of three-point bending fracture tests conducted on core-based concrete specimens with a chevron-type notch. The data obtained from fracture tests in the form of load vs. displacement and load vs. crack mouth opening displacement diagrams are analysed to obtain values for selected mechanical fracture parameters: modulus of elasticity E, fracture toughness K_{Ic}, and fracture energy G_F, which are determined based on the linear elastic fracture mechanics approach and Work-of-Fracture method. Within the study of the fracture behaviour of different materials, in recent years attention has been given to the use of X-ray imaging methods for the two-dimensional and three-dimensional characterization of internal structure and its alteration caused by various types of loading [7], of which the most modern approach is time-lapse X-ray computed tomography (4D-XCT) performed during fracture experiments [8, 9]. This method allows for the observation of changes in material structure caused by the loading process in three-dimensional models, and also supplements the determination of fracture parameters with data on the geometric and morphometric parameters of the damage that arises, which can be observed not only on the surface of the test specimen but also throughout its entire volume.

The article focuses on the options for obtaining as much information as possible about the material of existing structures while minimizing the size and number of samples taken from them and thus the damage caused to them as well. Tests were performed on cylindrical specimens with a chevron notch stress concentrator in the three-point bending configuration in order to determine modulus of elasticity, fracture toughness, and fracture energy. Further attention was paid to the determination of compressive strength values and their dependence on the slenderness of the core-drilled specimens in relation to the standardized L/D ratio [6, 10]. Selected specimens were tomographically monitored during the loading process, providing additional information on ongoing morphometric changes and damage propagation.

2. Materials and methods

2.1. Specimen sampling and preparation

For the experimental part, a collection of 27 specimens with a diameter of 50 mm was taken from the same cement-based concrete structure with the use of the diamond core drill method. For the standard compressive strength test, six groups of three specimens were prepared, each group differing in the length to diameter ratio (*L*/*D* ratio) of the specimens, which was set to 0.5, 1.0, 1.5, 2.0, 2.5, and 3.0.

For the determination of mechanical fracture parameters using the three-point bending test, a seventh group of three specimens were prepared with a length of 150 mm and equipped with a chevron-type notch. After the test, the ends of these specimens were used for complementary compressive strength tests as well.

The eighth and last group contained six specimens, each with a different *L*/*D* ratio conforming to the six ratios stated above, which underwent 4D-XCT scanning. These specimens were tomographically scanned twice – first in their initial state before loading, and then after applying the load. The numbers of samples in the groups subjected to different test methods, their labelling and nominal dimensions are listed in Table 1, while photographs of the specimens and their loading configurations are shown in figure 1.

Table 1. Groups of specimens and their nominal dimensions.

Group	Spec. (–)	Diameter (mm)	Length (mm)	*L*/*D* ratio (–)	Method
CN_05_1–3	3	50	25	0.5	Compressive strength
CN_10_1–3	3		50	1.0	Compressive strength
CN_15_1–3	3		75	1.5	Compressive strength
CN_20_1–3	3		100	2.0	Compressive strength
CN_25_1–3	3		125	2.5	Compressive strength
CN_30_1–3	3		150	3.0	Compressive strength
CN_L1–3	3		150	3.0	Three-point bending
CN_05–30_4X	6		diff.	diff.	X-ray tomography

2.2. Determination of mechanical fracture parameters

In this paper, the evaluated fracture experiment is a three-point bending test applied to cylindrical concrete specimens with a chevron-type notch. Load vs. midspan deflection diagrams (*F–d* diagrams) and load vs. crack mouth opening displacement diagrams (*F–CMOD* diagrams) were recorded during the specimen loading. The fracture tests were carried out using an electromechanical testing machine with a measuring range of 0−250 kN. The displacement increment was required to be constant − the speed of the induced displacement of the upper support was equal to 0.02 mm/min. A photograph of the test setup is shown in figure 1.

The above-mentioned recorded diagrams were used together with information about specimen dimensions, the cross-section and initial notch as input data for CheF academic software [11]. The values obtained for selected mechanical fracture parameters – modulus of elasticity E, fracture toughness K_{Ic}, toughness G_{Ic}, and fracture energy G_F – were determined based on the linear elastic fracture mechanics approach [1] and Work-of-Fracture method [12].

The first, almost linear part of the *F–CMOD* diagram (namely a selected point from this part with values F_i and corresponding $CMOD_i$) was used to estimate the modulus of elasticity E with the help of geometrical factor g_0 [13].

Figure 1. Specimens subjected to compressive and fracture tests. A) Photograph of the specimens. B) Illustration of the three-point bending fracture test setup with a chevron notched core-based concrete specimen. C) Illustrations of compressive tests.

$$E = g_0 \cdot \frac{F_i}{CMOD_i} \cdot \frac{1}{D},\ g_0 = 20.8 - 19.4 \cdot \frac{a_0}{D} + 142.3 \cdot \left(\frac{a_0}{D}\right)^2, \quad (1)$$

where D is specimen diameter, a_0 is the depth of the initial notch.

The maximum load F_{max} was used for fracture toughness K_{Ic} assessment with the help of geometrical factor A_{min} [14] and span length S:

$$K_{Ic} = A_{min} \cdot \frac{F_{max}}{D^{1.5}},\ A_{min} = \frac{S}{D} \cdot \left[1.835 + 7.15 \cdot \frac{a_0}{D} + 9.85 \cdot \left(\frac{a_0}{D}\right)^2\right] \quad (2)$$

The toughness G_{Ic} was then calculated as follows:

$$G_{Ic} = \frac{(K_{Ic})^2}{E}. \quad (3)$$

The work of fracture value W_F was assessed from the complete F–d diagrams [11]:

$$W_F = \int F(d)\mathrm{d}d, \quad (4)$$

and then the specific fracture energy G_F value was calculated:

$$G_F = \frac{W_F}{A_{lig}}, \quad (5)$$

where A_{lig} is the area of a ligament.

The following compressive tests were performed on the same electromechanical testing machine. The increment of the displacement was 0.05 mm/min. During the tests, the actual force and displacement of the upper girder were recorded directly from the testing machine's sensors. For the purpose of eliminating the effect of the testing machine's stiffness, the displacement of the loading plates was measured externally with the use of a pair of LVDT transducers. Three specimens from each *L/D* ratio group were used for the compressive test, which was applied until each specimen failed. The fourth specimen of each group was first scanned using X-ray computed tomography and then subjected to compressive testing. However, in these tests the specimens were not tested until failure occurred in order to maintain their integrity for the X-ray scan after the test. Thus, the maximum force applied to each scanned specimen was calculated as 90 % of the minimum force applied at the failure of the three specimens of each *L/D* ratio group tested previously. After a second X-ray scan, these specimens were loaded to failure. The last step of the experimental part of the investigation was to determine strength parameters via compressive tests on the adjusted ends of the specimens used earlier in the three-point bending tests. In the case of the specification of the relationship between the compressive strength and slenderness of concrete, these adjusted ends were set up in two more groups with *L*/*D* ratios of approximately 0.6 and 0.7, respectively.

The compressive strength was primarily determined from the performed compressive tests using the equation below.

$$f_c = \frac{F_{max}}{A_c}, \quad (6)$$

where F_{max} is the maximum force at the failure of the specimens, and A_c is the initial cross-section area of the specimens' loading surfaces.

2.3. X-ray computed tomography and the TORATOM device

Due to their ability to pass through opaque materials, X-rays are widely used to provide images of the internal structure of objects. Radiation is emitted from a generator (X-ray tube), passes through the examined object, where attenuation occurs proportional to the material characteristics of the object, and hits a detector, where 2D image information is generated. If a number (typically hundreds to thousands) of such images is acquired at different angles of rotation of the examined object relative to the generator-detector system, modern computational algorithms (e.g. filtered back projection) can reconstruct a three-dimensional model of this object, which can be handled further virtually without the need to manipulate the original specimen. Thus, industrial X-ray computed tomography (XCT) is considered to be a non-destructive method and is suitable, inter alia, for observing changes caused by various physical and chemical factors.

The advanced TORATOM (Twinned Orthogonal Adjustable Tomograph) device [15] depicted in figure 2 combines two X-ray tube–detector pairs in an orthogonal arrangement with a shared high-precision rotary tomographic table. This arrangement allows the use of imaging pairs individually but also simultaneously (dual-source or dual-energy XCT) during the data acquisition process for tomographic reconstructions. Projection magnification can be changed from about 1.2× to 100×. The device is designed modularly and allows, among other things, the quick exchange of various types of detectors available at the workplace. Concerning the type of detector used and its native pixel size, it is possible to change the resolution of CT reconstructions, i.e. the size of one spatial point of the model (voxel), from about 0.18 mm to micrometric. Very high stable resolution is achieved thanks to the use

of a fully motorized CNC-controlled positioning system mounted on an actively damped anti-vibration platform.

Six specimens with different *L*/*D* ratios were tomographically investigated in their initial state and after loading was applied up to 90 % of the previously determined compressive strength value. These conditions ensured that irreversible changes at the micrometric level were reflected in the structure of the material, but they stopped short of causing the specimen to fail. One specimen with an *L/D* ratio of 1.5 presented within this paper was additionally supplemented by tomography after the completion of the compressive strength test, e.g. after the maximum force was reached.

The specimens were scanned using one X-ray tube–detector pair. A Microfocus reflective-type X-ray tube (XWT-240-SE, X-Ray WorX, Germany) operating at an accelerating voltage of 230 kV and a target power of 48.3 W was used to generate the radiation. The projections were acquired by a flat panel detector (Dexela 1512NDT, Perkin Elmer, USA) with a GOS scintillator, a matrix of 1536 × 1944 pixels, a 74.8 μm pixel size and an active area of 114.9 × 145.4 mm.

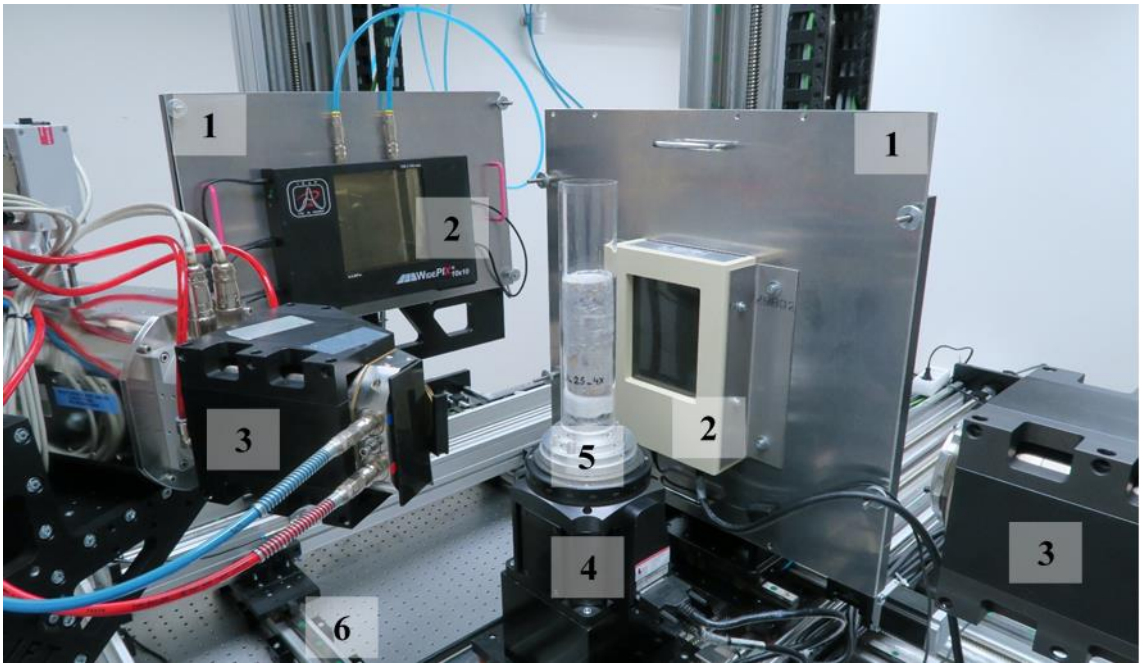

Figure 2. TORATOM tomography system with a concrete specimen: 1) Detector holder, 2) Detectors of different types, 3) X-ray tubes, 4) High-precision tomographic rotary stage, 5) Object under investigation, 6) Active damped anti-vibration table with CNC positioning system.

By setting the distance between the X-ray tube and detector to 359.6 mm and the distance between the X-ray tube and the specimen axis to 240.5 mm, a magnification of ~1.5× was obtained, leading to a voxel (one spatial point) size of ~50 μm in the resulting 3D volumetric models. However, due to the requirement for high resolution, the size of the active area of the detector was a limiting factor and for samples with an *L/D* ratio higher than 1.5 it was necessary to perform an XCT scan of each half of the sample separately and then virtually bind their models together. Thus, a total of 19 XCT scans were performed. For each scan, 1800 projections were taken as an average of 4 images with an exposure time of 230 ms.

Data treatment was performed using VG Studio Max (Volume Graphics, Germany) and the free open-source software ImageJ. After the reconstruction of virtual 3D models using logarithmization and a filtered back-projection algorithm, the time-lapse models were mapped to each other by rigid transformations. To be able to monitor the changes, differential models between the initial and final state were calculated. From this difference, it was possible to segment the cracks, observe their pattern

and determine their geometric parameters (including the fractal dimension) by applying the box-counting algorithm embedded in the BoneJ plugin in ImageJ free open-source software [16]. Furthermore, the size and direction of displacements were calculated based on local non-linear transformations using a digital volume correlation module embedded in VG Studio Max.

3. Approximation of the strength factor

Approximation of the strength factor [17] was carried out during the derivation of an updated simplified analytical model of the compressive strength of a concrete specimen similar to that found in [18].

3.1. Derivation of the root of approximation

The assumption is that the main crack will only slightly deviate from a plane. Such a plane will have an angle α according to a plane perpendicular to the cylinder axis. The strength factor c can then, by taking a simplified model into account, be approximated by a relationship:

$$c_{\mathrm{root}}(L/D) = \frac{1}{sin\alpha} = \frac{\sqrt{D^2+L^2}}{L} = \frac{\sqrt{1+(L/D)^2}}{L/D} = \sqrt{\frac{1+(L/D)^2}{(L/D)^2}}. \tag{7}$$

3.2. Generalization of the approximation

The relationship (7) can be parametrized by adding a variable exponent p, which helps with the empirical data fit:

$$c_{\mathrm{p}}(L/D) = \sqrt{\frac{1+(L/D)^p}{(L/D)^p}}, \tag{8}$$

for which the value of $p = 3$ will be used here.

However, concrete specimens tend to have a slightly lower steepness, which the following update takes into account:

$$c(L/D) = q\left(\sqrt{\frac{1+(L/D)^p}{(L/D)^p}} - 1\right) + 1, \tag{9}$$

where $q = 0.7$ is the steepness parameter (which is reduced by 30 % according to (8)).

The measured compressive strength is then given by the expression:

$$f_{\mathrm{c}}(L/D) = c \cdot f_{\mathrm{ca}}, \tag{10}$$

where f_{ca} is the asymptotic value of compressive strength, which is assumed to be independent of the length L of the specimen.

4. Results

4.1. Fracture parameters obtained from three-point bending tests

The following table illustrates the results gained from the aforementioned three-point bending tests. The fundamental geometry values of the specimens along with their mechanical fracture parameters such as modulus of elasticity, fracture toughness, fracture energy, etc. are shown in table 2: measured values, mean values, standard deviations (StDev), and coefficients of variation (CoV).

Table 2. Cylinder bending specimens with a chevron notch: input and outputs.

	Parameter	Symbol	Specimen			Mean	StDev	Unit	CoV (%)
			CN_L1	CN_L2	CN_L3				
Inputs	Diameter of specimen	D	49.73	49.67	49.72	49.70	0.03	mm	0.1
	Notch tip depth	a_0	3.50	3.47	3.93	3.63	0.26	mm	7.1
	Notch depth	h_0	9.88	9.36	10.01	9.80	0.35	mm	3.5
	Span of specimen	S	140.0	140.0	140.0	140.0	0.0	mm	0.0
Outputs	Modulus of elasticity	E	21.7	22.2	15.1	19.7	3.94	GPa	20.0
	Critical stress intensity factor	K_{Ic}	0.755	0.679	0.859	0.764	0.090	$MPa \cdot m^{1/2}$	11.8
	Critical energy release	G_{Ic}	26.3	20.8	48.7	31.9	14.8	$N \cdot m^{-1}$	46.3
	Fracture energy	G_F	103.2	128.2	167.4	132.9	32.39	$J \cdot m^{-2}$	24.4
	Fracture energy ratio	G_F/G_{Ic}	3.93	6.16	3.43	4.50	1.45	–	32.2

4.2. Fracture parameters and their relation to the slenderness ratio

In table 3, values obtained from compressive strength tests on specimens with different length to diameter ratios are shown. Besides the values from the tests for each specimen, the results include mean compressive strength and CoV values for each group of specimens.

Table 3. Results of the compressive tests.

Specimen	Diameter	Length	Length to diameter ratio	Density	Maximal force	Compressive strength	
	D	L	L/D	D_c	F_{max}	f_c	
	(mm)	(mm)	(–)	$(kg \cdot m^{-3})$	(N)	$(N \cdot mm^{-2})$	
CN_05_1	49.73	25.55	0.51	2269	162840	**83.8**	$f_{c,mean}$
CN_05_2	49.67	25.69	0.52	2284	169650	**87.6**	83.1
CN_05_3	49.73	25.68	0.52	2282	152960	**78.8**	CoV (%)
CN_05_4X	49.70	25.53	0.51	2293	159726	**82.3**	4.4
CN_10_1	49.77	50.50	1.01	2315	93370	**48.0**	$f_{c,mean}$
CN_10_2	49.77	50.03	1.01	2277	94820	**48.7**	45.8
CN_10_3	49.79	50.42	1.01	2295	85430	**43.9**	CoV (%)
CN_10_4X	49.74	50.54	1.02	2278	82922	**42.7**	6.5
CN_15_1	49.72	75.19	1.51	2294	73330	**37.8**	$f_{c,mean}$
CN_15_2	49.77	74.85	1.50	2302	72890	**37.5**	39.1
CN_15_3	49.76	75.40	1.52	2291	80180	**41.2**	CoV (%)
CN_15_4X	49.80	75.34	1.51	2293	77950	**40.0**	4.6

Table 4. Results of the compressive tests (cont.).

Specimen	Diameter	Length	Length to diameter ratio	Density	Maximal force	Compressive strength	
	D	L	L/D	D_c	F_{max}	f_c	
	(mm)	(mm)	(–)	(kg·m^{-3})	(N)	(N·mm^{-2})	
CN_20_1	49.81	100.82	2.02	2283	71620	**36.8**	$f_{c,mean}$
CN_20_2	49.72	99.34	2.00	2279	76520	**39.4**	37.3
CN_20_3	49.64	99.73	2.01	2300	74400	**38.4**	CoV (%)
CN_20_4X	49.74	99.86	2.01	2285	67135	**34.6**	5.7
CN_25_1	49.65	125.75	2.53	2256	69510	**35.9**	$f_{c,mean}$
CN_25_2	49.63	124.30	2.50	2266	76730	**39.7**	36.9
CN_25_3	49.74	123.32	2.48	2289	70010	**36.0**	CoV (%)
CN_25_4X	49.73	124.47	2.50	2296	70156	**36.1**	5.0
CN_30_1	49.71	149.65	3.01	2317	68430	**35.3**	$f_{c,mean}$
CN_30_2	49.68	149.95	3.02	2303	65540	**33.8**	36.0
CN_30_3	49.76	149.99	3.01	2287	73200	**37.6**	CoV (%)
CN_30_4X	49.75	149.68	3.01	2273	72467	**37.3**	5.0

Additionally, compressive strength values obtained from the adjusted ends of specimens previously used for the three-point bending test are shown in table 4.

Table 5. Results of the compressive tests performed on the adjusted ends of specimens after the three-point bending test.

Specimen	Diameter	Length	Length to diameter ratio	Density	Maximal force	Compressive strength	
	D	L	L/D	D_c	F_{max}	f_c	
	(mm)	(mm)	(–)	(kg·m^{-3})	(N)	(N·mm^{-2})	
CN_L1a	49.76	62.98	1.27	2264	84150	**43.3**	$f_{c,mean}$
CN_L1b	49.72	63.10	1.27	2257	62290	**32.1**	36.8
CN_L2a	49.75	63.35	1.27	2273	78000	**40.1**	
CN_L2b	49.74	54.43	1.09	2634	71580	**36.8**	CoV (%)
CN_L3a	49.76	63.30	1.27	2286	67500	**34.7**	11.4
CN_L3b	49.74	63.43	1.28	2282	65930	**33.9**	

Figure 3 shows a graphical illustration of the gained values for compressive strength and L/D ratio for each tested group of specimens, including the adjusted specimens after the three-point bending test. These values are supplemented by the cube compressive strength value of the same concrete tested in the form of drilled core specimens. Besides these results, data from the experiment were used for the calculation of the asymptotic value f_{ca} = 34.95 N·mm^{-2} of the approximation function (10) by the least squares method. A comparison of the values of the approximation function and correction factors from EN 12390-3 [6] and ASTM C42/C42M [10] is shown in figure 4.

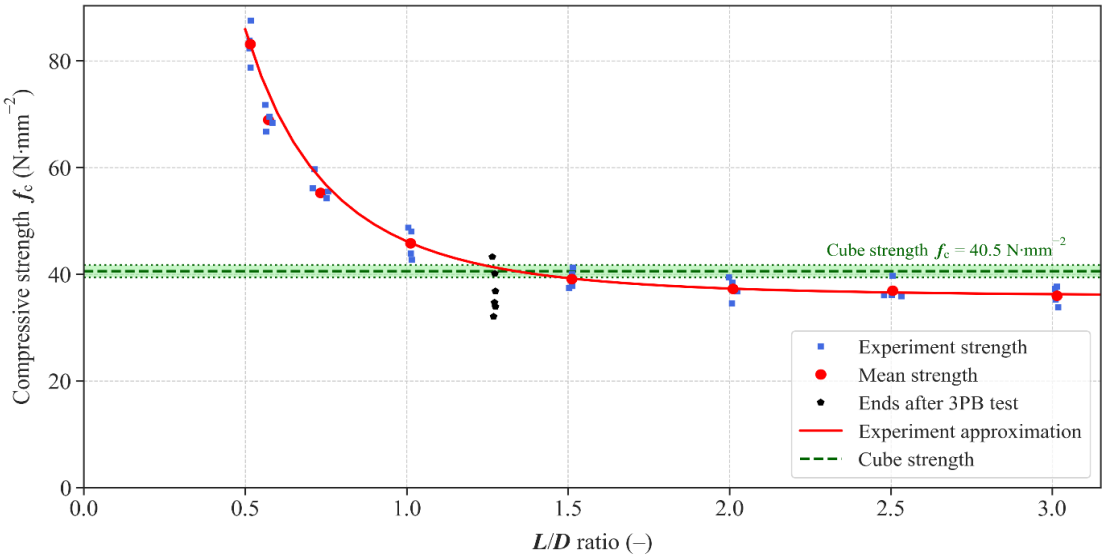

Figure 3. Results obtained from compressive tests. The plot shows the relationship between the compressive strength and the *L*/*D* ratio. In addition, the cube strength and approximation function of the experiment are shown.

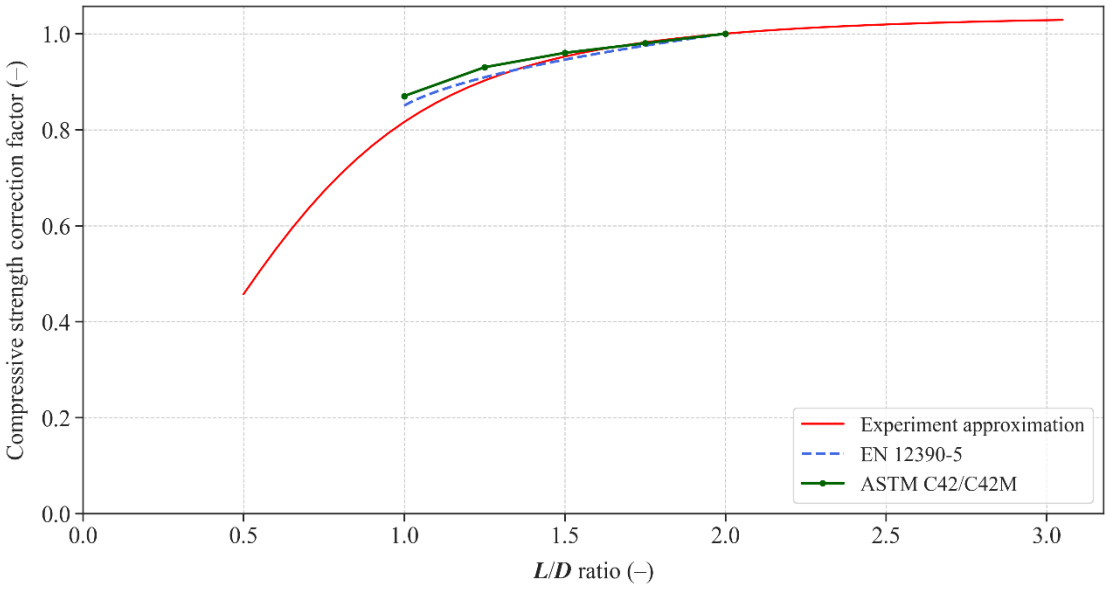

Figure 4. Approximated function and functions from existing codes and recommendations for the compression strength correction factor with relation to the *L*/*D* ratio of concrete specimens.

4.3. Tomographic observation and volume analyses

From the qualitative assessment of the computed tomography results in figure 5, it is obvious that the initiation of cracks within the volume at 90 % of the minimum force at failure is difficult to observe and differences in comparison with the initial state are not clearly visible until the maximum force is reached and damage propagates. Although the given resolution plays a major role in the detectability and visibility of the expected microcracks, these are additionally hidden in the distinctive structure of the

material. Thus, differential volumes were used to monitor the cracks' pattern, their segmentation and the determination of geometric parameters. These volumes, represented by an example slice in figure 6, were calculated as the difference of virtual models rigidly transformed to geometrically match as much as possible. Based on digital volume correlation displacement fields, e.g. directions and magnitudes were calculated.

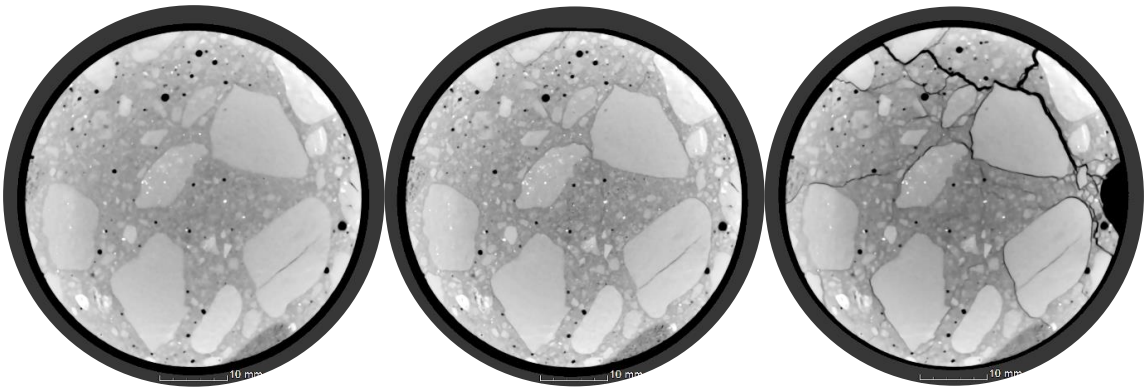

Figure 5. Tomographic slices in the middle of the specimen length oriented parallel to the base. From the left: specimen in its initial state, specimen at 90 % of the minimum force at the failure measured at the same *L/D* ratio, specimen after failure.

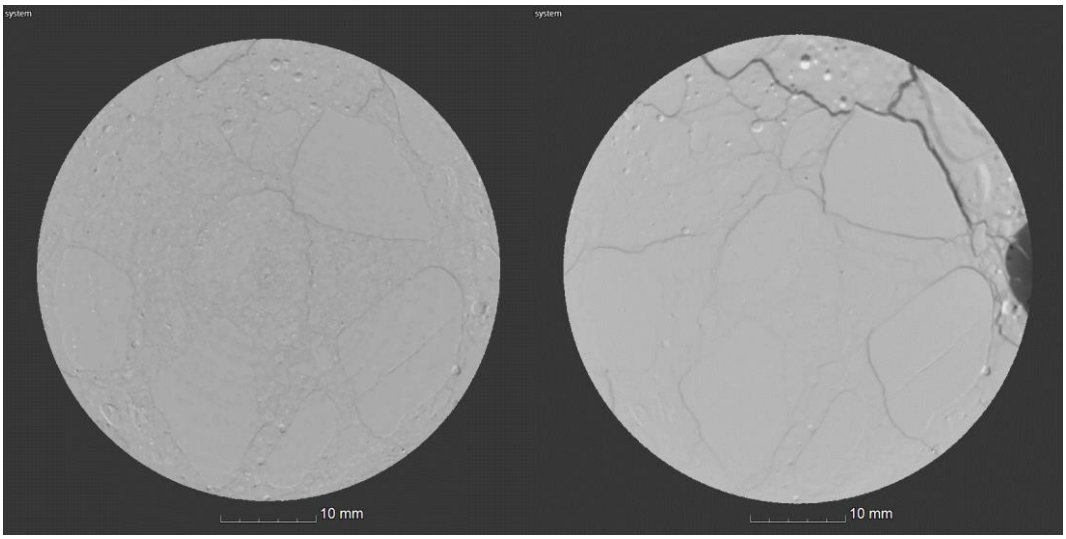

Figure 6. Differential tomographic slices from the middle of the specimen length oriented parallel to the base. Left: the difference between the specimen in its initial state and the specimen at 90 % of the minimum force at failure; right: the difference between the specimen in its initial state and the specimen after failure.

Different 3D representations of the obtained results are shown in figure 7. In the first column, there is a section of the specimen representing the changes to the initial state. The colour coding corresponds to the intensity values normalized to their standard deviation from –0.5 to 1.5. In the second column, there is a section of the specimen representing the displacement magnitude fields. In the third column displacement lines representing the directions of the displacement are provided. The colour coding here corresponds to a displacement from 0 to 1.5 mm. In the fourth column, a red crack pattern is visualised within the grey specimen body.

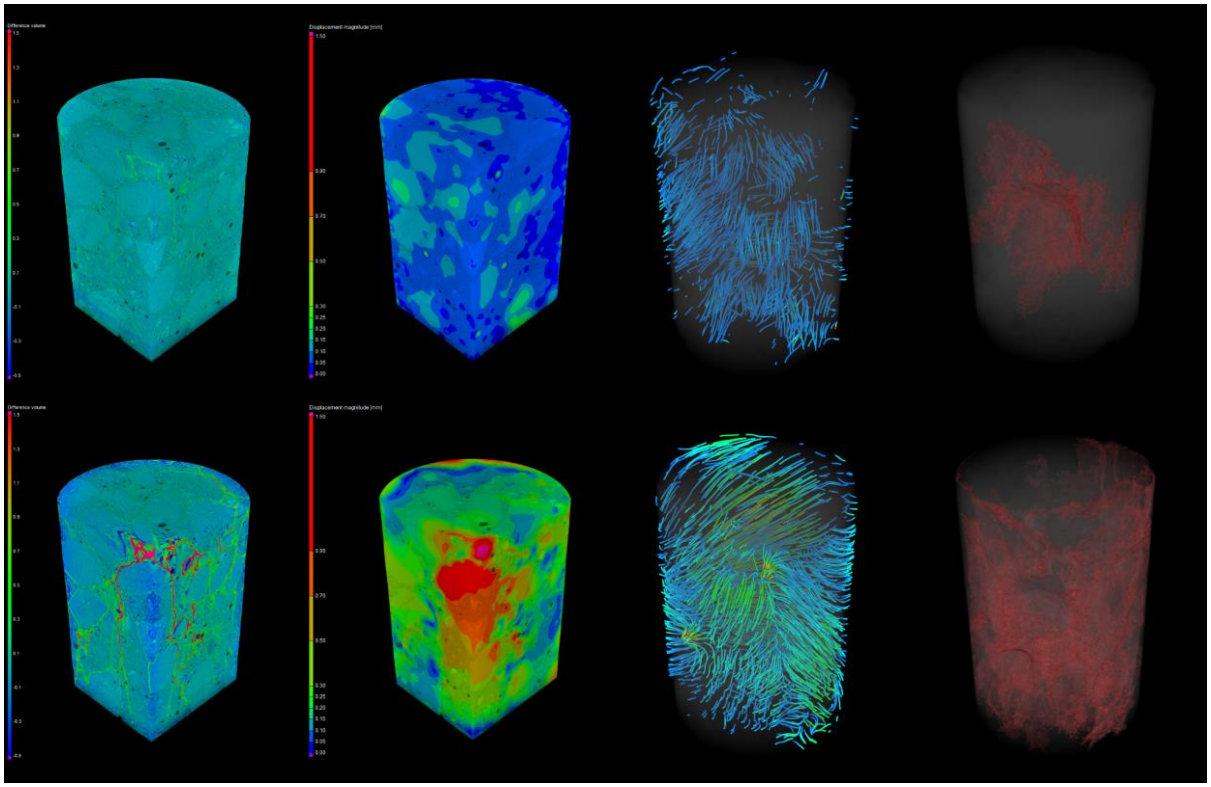

Figure 7. 3D representations of the CT results. Top row: specimen at 90 % of the minimum force at failure; bottom row: specimen after failure. From the left: volume changes compared to the initial state, displacement magnitude, displacement lines, 3D crack pattern.

Table 6. Values obtained based on computed tomography results.

Specimen CN_15_4X state / Volume analyses and characteristics	Initial state	90 % of the minimum force at failure	After failure
Material volume (mm^3)	123169.29	123038.88	119527.45
Void volume, incl. pores (mm^3)	1606.15	1684.90	7710.62
Crack volume (mm^3)	–	939.46	6351.74
Void volume fraction, incl. pores (%)	1.29	1.35	6.06
Crack volume fraction (%)	–	0.75	4.99
Crack volume surface (mm^2)	–	15591.26	67467.10
Displacement magnitude max (µm)	–	1300.00	2733.30
Displacement magnitude mean (µm)	–	77.60	365.30
Displacement magnitude median (µm)	–	73.50	205.54
Crack fractal dimension D (–)	–	2.1129	2.2756
Coefficient of determination R^2 (%)	–	99.9978	99.9931

From the values determined based on the volumetric data summarized in table 6, additional information can be deduced. At 90 % of the minimum force at failure when relatively high displacement values are already being recorded, the material loss and void volume increase is minimal, which indicates the thinning of the material in the interfacial transition zone and the initiation of microcracks among the present pores. However, after failure the material loss is significant and the crack coincides with the present pores. In both cases, the values for the content of the fracture surface are relatively high and the cracks are richly branched, as is also evidenced by the fractal dimension value.

5. Discussion

The influence of the length to diameter (L/D) ratio on the compressive strength of concrete is not negligible. In order to evaluate tested concrete and make further use of compressive strength values it is necessary to know the cube or cylindrical compressive strength which is used by default. This means that the used samples taken from the structure must have specific dimensions, e.g. length to diameter ratio. In some cases, it is difficult to adhere to the required dimensions and so it is desirable to know the relationship between compressive strength and the L/D ratio. The performed compressive strength tests show the effect of slenderness ratio on the resulting compressive strength of concrete specimens. Specimens with a slenderness ratio lower than 1.0 show considerable higher compressive strength than specimens with a higher L/D ratio.

Some codes and requirements contain values for a correction factor that allows the recalculation of the compressive strength value obtained for concrete specimens according to the ratio of their slenderness to cube strength (L/D = 1.0) or cylindrical strength (L/D = 2.0) [6, 10]. However most of these values from codes and requirements are specified only in the range from 1.0 to 2.0 due to the above-mentioned need to recalculate only specimens in this range. The supplementation of the code correction factors with the correction factor gained from the approximation shown in figure 4 can help to correct the compressive strength values obtained for specimens of dimensions other than those which are recommended by the standards. This can reduce the core-drilled specimens needed, both in terms of dimensions and numbers.

The specimens made from halves left over after the three-point bending test reached lower compressive strength values than expected. This difference could be caused by multiple saw-cutting (notch cutting, adjusting the specimens for the compressive strength test) that caused damage to the microstructure of the concrete.

The complementary performance of tomographic observation and volume analyses allows the observation of changes in material structure caused by the loading process in three-dimensional models and supplements the determination of fracture parameters with additional knowledge of the geometric and morphometric parameters of the arising damage. The tomographic virtual model can also serve as an input or comparison for modelling and predicting the fracture behaviour of the studied material.

6. Conclusion

The mechanical fracture parameters of concrete drill-core specimens and the response of their internal structure to load with regard to the slenderness ratio have been studied in this paper. Eight groups of concrete core-drilled specimens with various L/D ratios were set up and the influence of the L/D ratio on the compressive strength was specified. The results of compressive tests were used for the creation of an approximation function which specifies the influence of the specimen's slenderness on its compressive strength. Three-point bending tests were performed to determine the fracture characteristics of the used concrete, and selected specimens were analysed and three-dimensionally characterized via high-resolution X-ray computed tomography.

In the case of diagnostics and concrete structure evaluation, the amount of taken samples is crucial, and it is desirable to obtain as many values for material characteristics as possible from a single specimen. One of the options is to use the same sample of concrete for more tests, such as in this paper – specimens were subjected to three-point bending tests, and then their adjusted halves that remained

after such testing underwent compressive strength tests. The paper also describes the combination of compressive strength tests and X-ray computed tomography.

It has been shown that specimens with a lower *L*/*D* ratio reached higher compressive strength values than specimens with a higher *L*/*D* ratio – the advanced approximation derived from an analytical model of the compressive strength of a concrete specimen perfectly fitted into the whole range of slenderness ratios. In future research the influence of the method of cutting and preparing the samples on the mechanical properties of the concrete could be determined, as well as the more detailed relationship between the slenderness of specimens and the compressive strength of concrete with an *L*/*D* ratio ranging from 0.5 to 2.0.

7. References

[1] Karihaloo B L 1995 Fracture mechanics and structural concrete (New York: Longman)
[2] Shah S P, Swartz S E and Ouyang Ch 1995 Fracture mechanics of structural concrete: applications of fracture mechanics to concrete, rock, and other quasi-brittle materials (New York: Wiley)
[3] Bažant Z P and Planas J 1998 Fracture and Size Effect in Concrete and other Quasibrittle Materials (Boca Raton: CRC Press)
[4] European Committee for Standardization EN 13791 2019 Assessment of In-situ Compressive Strength in Structures and Precast Concrete Components
[5] Panizza M, Natali M, Garbin E, Ducman V and Tamburini S 2020 Optimization and mechanical-physical characterization of geopolymers with Construction and Demolition Waste (CDW) aggregates for construction products *Construction and Building Materials* **264**
[6] European Committee for Standardization EN 12390-3 2020 Testing Hardened Concrete – Part 3: Compressive strength of test specimens
[7] Trawinski W, Bobinski J and Tejchman J 2016 Two-dimensional simulations of concrete fracture at an aggregate level with cohesive elements based on X-ray μCT images *Engineering Fracture Mechanics* **168** pp 204–26
[8] Skarzynski L and Tejchman J 2016 Experimental Investigations of Fracture Process in Concrete by Means of X-ray Micro-Computed Tomography *Strain* **52** pp 26–45
[9] Kumpova I, Vopalensky M, Fila T, Kytyr D, Vavrik D, Pichotka M, Jakubek J, Kersner Z, Klon J, Seitl S and Sobek J 2018 On-the-Fly Fast X-Ray Tomography Using a CdTe Pixelated Detector – Application in Mechanical Testing *IEEE Transactions on Nuclear Science* **65** 2870–76
[10] ASTM International 2012 ASTM C42 / C42M-12 Standard Test Method for Obtaining and Testing Drilled Cores and Sawed Beams of Concrete ASTM International West Conshohocken PA
[11] Svobodová B, Šimonová H and Keršner Z 2018 Calculation of Mechanical Fracture Parameters of Chevron Notched Core Based Concrete Specimen: Software CheF. In Solid State Phenomena: *24th Concrete Days 2017*. Solid State Phenomena. Switzerland: Trans Tech Publications pp 185–188
[12] RILEM TC-50 FMC (Recommendation) 1985 Determination of the fracture energy of mortar and concrete by means of three-point bend test on notched beams, *Materials & Structures* **18** pp 285–290
[13] Backers T 2004 Fracture toughness determination and micromechanics of rock under mode I and mode II loading, dissertation thesis, University of Potsdam
[14] Ouchterlony F 1988 Suggested methods for determining the fracture toughness of rock, Int. J. *Rock Mech. Min. Sci. & Geomech. Abstr.* **25** pp 71–96
[15] Fila T and Vavrik D 2016 A multi-axial apparatus for carrying out X-ray measurements, particularly computed tomography. European patent No. 14002662.6
[16] Doube M, Kłosowski M M, Arganda-Carreras I et al 2010 Bonej: Free and extensible bone image analysis in ImageJ *Bone* **47**(6) pp 1076–79

[17] Frantík P 2021 Approximation of compressive strength of concrete specimen, published online at http://www.kitnarf.cz/publications/2021/2021.06.www_fc_approx/2021.06.www_fc_approx.pdf
[18] Frantík P 2005 Simple model of compressive fracture (in Czech) Proceedings of seminars *Problémy lomové mechaniky* V. Brno

Acknowledgement
The research was carried out as part of the Brno University of Technology specific university research project No. FAST-J-21-7473, with the support of the Czech Science Foundation under project 19-09491S (MUFRAS) and a project for the long-term conceptual development of research organizations, RVO 68378297.